A Novel Tantalum-Containing Bioglass. Part I. Structure and Solubility

Adel MF Alhalawani

Mark R. Towler
Missouri University of Science and Technology, mtowler@mst.edu

Recommended Citation

A novel tantalum-containing bioglass. Part I. Structure and solubility

CrossMark

Adel MF. Alhalawani [a], Mark R. Towler [a,b,*]

[a] Department of Mechanical & Industrial Engineering, Ryerson University, Toronto, Ontario, Canada
[b] Li Ka Shing Knowledge Institute, St. Michael's Hospital, Toronto, Ontario, Canada

A B S T R A C T

Bioglasses are employed for surgical augmentation in a range of hard tissue applications. Tantalum is a bioactive and biocompatible transition metal that has been used as an orthopedic medical device. It has a range of biological and physical properties that make its incorporation into ionic form into bioactive glass systems promising for various clinical applications. The work herein reports the characterization and properties of novel tantalum-containing glasses. A series of glasses based on the system $48SiO_2\text{-}(36\text{-}X)ZnO\text{-}6CaO\text{-}8SrO\text{-}2P_2O_5\text{-}XTa_2O_5$ with X varying from 0 mol% (*TA0*) to 0.5 mol% (*TA2*) were synthesized. The addition of small amounts of Ta_2O_5 did not cause crystallization of the glasses but increasing Ta_2O_5 content at the expense of ZnO was found to result in an increased number of bridging oxygens (BOs). This, along with the data recorded by differential thermal analysis (DTA) and magic angle spinning-nuclear magnetic resonance (MAS-NMR), confirms that Ta acts as a glass former in this series. Solubility experiments showed that minor changes in the glass structure caused by Ta incorporation (0.5 mol%) exhibited greater cumulative % weight loss, pH values and cumulative Zn^{2+} and Sr^{2+} ion concentration over a period of 30 days of maturation, when compared to Ta_2O_5-free glasses. The results presented in this article confirm that replacing ZnO with Ta_2O_5 in silicate glasses results in the formation of stronger bonds within the glass network without any adverse effects on the solubility of the glasses prepared from them.

© 2016 Elsevier B.V. All rights reserved.

1. Introduction

Bioactive glasses are candidate materials for a wide variety of biomedical applications as they can bond to bone and be formulated to release bioactive ions into the local environment, resulting in antimicrobial activity and enhanced cell response [1,2].

Silicate-glasses are inorganic amorphous solids composed of SiO_4^{3-} tetrahedral units. In other words, silicon is coordinated to 4 oxygen atoms and each oxygen atom is coordinated to 2 silicon units so that the structure is a three-dimensional (3-D) network of corner connected $[SiO_{4/2}]$ tetrahedra [3]. These SiO_4^{3-} tetrahedral units form the backbone of the glass structure while modifying cations charge balance the silicate chains. The ionicity of the Si—O bond, resulting from the difference in the electronegativity of Si and O, allows for the formation of Si—O—Si bonds [4], forming the backbone of various bioglass systems. Si can also bond to other atoms depending on the glass composition [5,6]. Indeed, bond formation corresponds to a state of electronegativity equalization stated by Sanderson [7]. When a bond is formed between two atoms, X and Z, with different electro-negativities, there is an electron flow from the less to the more electronegative atom. Further, it is accepted that silica glasses undergo modification in response to the addition of other cations/atoms [8]. As an example, the alkali ions locate themselves in the structure near the non-bridging oxygen (NBO) when added to silica glasses resulting in the formation of meta, pyro and ortho-silicates. $[SiO_{4/2}]^0$, $[SiO_{3/2}O]^-$, $[SiO_{2/2}O_2]^{2-}$, $[SiO_{1/2}O_3]^{3-}$ and $[SiO_4]^{4-}$, which are present in silicate glasses, are designated as Q^4, Q^3, Q^2, Q^1 and Q^0 respectively, where the superscripts indicate the number of bridging oxygens (BOs) centered on the given Si atom through which it is connected to other Si atoms in the glass structure [9].

The solubility of a bioglass network is related to alkali ion content [9]; the addition of glass former cations will result in a systematic decrease in the solubility of these systems. Readers are referred to the work of Hoppe et al. [1] for detailed information on the degradation kinetics of these biomaterials and the specific effect of the released ionic dissolution products, for example Sr^{2+} and Zn^{2+} ions, impart on biological performance.

Transition metals can play a dual role in oxide glasses [10]. In some concentrations the transition metal may enter the network structure while in other concentration amounts, they may allow the oxygen ions of their former cation to break the oxygen bridges in the system, therefore acting as a glass modifier. Tantalum (Ta) is a transition metal that has been used as a bone implant [11–13] due to its physical and biological properties. The Ta ion is reported to be bioactive and

* Corresponding author at: Department of Mechanical and Industrial Engineering, Faculty of Engineering and Architectural Science, 350 Victoria Street, Toronto M5B 2K3, ON, Canada.
E-mail address: mtowler@ryerson.ca (M.R. Towler).

biocompatible due to the formation of a stable tantalum pentoxide (Ta_2O_5) component on its surface [14,15]. Studies [11,16] have shown that Ta surfaces exhibit lower contact angles and higher surface energies than titanium (Ti) or hydroxyapatite (HA) surfaces offering a favorable biological environment for adhesion, growth and differentiation of human cells. Despite some processing challenges [13,17], the inclusion of Ta and other transition metals into ionomer glasses can improve their thermal and chemical stability [6,18–20].

In a previous article [6], the authors synthesized and characterized a wholly new silicate-glass series in which ZnO was substituted with up to 8 mol% Ta_2O_5. In that work, Alhalawani and Towler showed that Ta incorporation into silicate-based glasses was possible by the melt-quenching process. They also confirmed that Ta behaved as a glass former whereas Zn acted as a glass intermediate, depending on its content, in that particular glass system. These novel glasses were designed specifically to formulate a series of glass polyalkenoate cements (GPCs) for use in sternal fixation. Initial, unpublished data has confirmed that high Ta-containing glasses have rheology (setting and working times) that are deemed unsuitable for sternal applications. The work herein expands the understanding of this particular bioglass system where a new series of the previously formulated glass [6] was synthesized containing lower Ta_2O_5 contents (0.0 to 0.5 mol%). The manuscript also aims to characterize the structure and solubility of the glass system under study.

2. Experimental methods

2.1. Glass synthesis

Three glasses were proposed for this study (Table 1), a Ta_2O_5-free SiO_2-ZnO-CaO-SrO-P_2O_5 glass (*TA0*) and two Ta_2O_5-containing glasses (*TA1* and *TA2*). Appropriate amounts of analytical grade silica, zinc oxide, calcium carbonate, strontium carbonate, ammonium dihydrogen phosphate and tantalum oxide (Fisher Scientific, Ottawa, ON, Canada; Sigma-Aldrich, Oakville, ON, Canada) were weighed out and hand-mixed using a spatula. Platinum (Pt.) crucibles and a Lindberg/Blue M model furnace (Lindberg/Blue M, Asheville, NC USA) with a UP550 controller were used for melting the sieved powders (1650 °C, 1.5 h). The melts were shock quenched in water to obtain frit which was then dried in an oven (100 °C, 1 h), ground using a ball mill (400 rounds per minute, 15 min), and sieved once more through a 45 μm mesh. *TA0*, *TA1* and *TA2* were then annealed at 670 °C, 666 °C and 677 °C, respectively for 12 h to relieve internal stresses within the glass network. The furnace (Lindberg/Blue M, Asheville, NC, USA) was programmed to reach to the annealing temperature in 3 h and to cool down to the room temperature (25 ± 2 °C) in 3 h. The glass powders of the selected compositions were then sieved through a 45 μm mesh and utilised for subsequent characterization.

2.2. Glass structural and thermal characterization

2.2.1. X-ray diffraction (XRD)

A Bruker D2 Phaser desktop X-ray diffractometer (Bruker AXS Inc., WI, USA) was used to obtain X-ray diffraction patterns from the glasses at room temperature (23 ± 1 °C). Glass powder samples were packed into stainless steel sample holders. With the X-ray generator set at 30 kV and 30 mA, a copper anode was used to produce a divergent beam with an average Kα wavelength of 1.541874 Å. The range of 10–80° 2θ with a step size of 0.02° 2θ and a count time of 10 s per step were used for the measurements. X'Pert Highscore™ data analysis software version 1.0 d (PANalytical, Almelo, The Netherlands) was employed to find peak parameters.

2.2.2. Particle size analysis (PSA)

The particle size distribution (PSD) of each glass series was recorded using a Multisizer 4 Particle size analyzer (Beckman Coulter, Fullerton, CA, USA). The glass powder samples ($n = 5$) were evaluated in the range of 2 to 60 μm with a run length of 60 s. A background analysis was performed and subtracted for accurate results. The fluid used in this case was a sodium chloride (NaCl) electrolyte solution at a temperature range of 10–37 °C. The relevant volume statistics were calculated on each glass composition. The average diameters ($n = 5$) at the 10%, 50%, and 90% of the cumulative volume distribution (d_{10}, d_{50} and d_{90}, respectively) were recorded.

2.2.3. Scanning electron microscopy-energy dispersive spectroscopy (SEM-EDS)

Sample imaging was carried out with an FEI Co. Quanta 200F Environmental Scanning Electron Microscope equipped with an EDAX Genesis Energy-Dispersive Spectrometer (Oxford Instruments X-max, Netherlands). Secondary electron (SE) and backscattered electron (BSE) images were taken on glass particles and polished disc surfaces. All EDS spectra were collected at 20 kV using a beam current of 26 nA. Quantitative EDS spectra was subsequently converted into relative concentration data ($n = 3$).

2.2.4. Differential thermal analysis (DTA)

A combined differential thermal analyzer–thermal gravimetric analyzer (DTA–TG; SDT 2960 Simultaneous DSC-TGA, TA Instruments, DW, USA) was used to study the thermal properties of the glasses. A heating rate of 20 °C/min was employed using an air atmosphere with alumina in a matched platinum crucible as a reference and then cooled to room temperature at the same rate. Sample measurements were carried out every 6 s between 30 °C and 1200 °C. Data analysis was performed using NETZSCH Proteus software, V. 6 (Netzsch-Gerätebau GmbH, Selb, Germany).

2.2.5. X-ray photoelectron spectroscopy (XPS)

The powders' chemical compositions as well as local chemical environment were analyzed using PHI Quantera Scanning X-ray photoelectron Microprobe (XPS). The XPS data sets were collected with Al Kα X-rays (monochromatic, beam size = 100 μm) at an output power of 26.2 watts, with a photon energy of 1486.6 eV and a step size of ~0.025 eV. Survey scans (~0.5 eV step size) were performed with a pass energy of 140 eV to gain qualitative information such as peak identification and peak position. Peaks identified in all survey scans were used to adjust high resolution scan binding energy range, pass energy (26 eV) and beam dwelling time (~100 ms). The beam sweeps for each high resolution scan was adjusted to yield a signal-to-noise ratio of >100:1. The analyzed area was 1–2 mm in diameter.

2.2.6. Magic angle spinning-nuclear magnetic resonance (MAS-NMR)

^{29}Si MAS-NMR spectra were recorded at 7.05 T (Tesla) on a Varian Unity Inova 300 FT-NMR spectrometer (Palo Alto, CA, USA), equipped with a cross polarization-magic angle spinning (CP-MAS) probe. The glass samples were placed in a zirconia sample tube with a diameter of 7 mm. The sample spinning speed at the magic angle to the external magnetic field was 5 kHz. ^{29}Si MAS NMR spectra were taken at 59.59 MHz with 7.0-ls pulse length (pulse angle, p/2), 100-s recycle delays, where the signals from 2126, 1837 and 1880 pulses were

Table 1
Composition of the glass series.

	SiO_2	ZnO	CaO	SrO	P_2O_5	Ta_2O_5
mol%						
TA0	48.0	36.0	6.0	8.0	2.0	0.0
TA1	48.0	35.8	6.0	8.0	2.0	0.2
TA2	48.0	35.5	6.0	8.0	2.0	0.5
wt%						
TA0	35.8	36.4	7.5	14.7	5.7	0.0
TA1	35.5	35.8	7.4	14.5	5.7	1.1
TA2	35.0	35.1	7.3	14.3	5.6	2.7

accumulated for *TA0*, *TA1* and *TA2*, respectively. ^{29}Si NMR chemical shifts are reported in ppm, with PDMS (polydimethyl silane) as the external reference (−34 ppm vs. TMS 0 ppm). All NMR spectra were recorded in a room for exclusive use of NMR, where the room temperature was kept at 300 K by means of an air-conditioner. Data analysis of the NMR spectra was performed by nonlinear curve-fitting using ORIGIN software (Microcal Software Inc., Northhampton, MA, USA).

2.3. Effect of glass structure on ion release and solubility

2.3.1. Disc sample preparation and degradation analysis

Disc samples were prepared by weighing 0.1 g powder into a stainless steel die (sample diameter 1.5×6 mm ϕ) which was pressed under 2.5 tons of pressure for 30 s. Disc samples were kept amorphous by annealing at $T_g \pm 10$ °C for 12 h. The surface area of each glass disc was then calculated from the dimensions measured using an electronic precision caliper (Cedarlane Laboratories Ltd., Hornby, ON, Canada). Disc samples were then weighed and immersed in measured quantities (10 ml) of de-ionized (DI) water. All samples were maintained at 37 °C. At various time points (1, 7 and 30 days), the DI water was removed for pH and ion release analysis. Then the discs were removed, dried in an incubator for 24 h, and weighed before being immersed in fresh volumes of DI water. This study was conducted in triplicate, and the data plotted as cumulative degradation (percentage weight loss per unit area, as a function of time). Eq. (1) was then used to obtain the % weight loss per unit area:

$$\% \text{ of weight loss} = \frac{M_o - M_t}{A} \times 100 \qquad (1)$$

where M_o is the initial weight in g, M_t is the weight at time t in g and A is the surface area in cm^2.

2.3.2. pH analysis

The pH measurements were collected using a Corning 430 pH meter (Corning Life Sciences, Acton, MA). Prior to testing, the pH electrode was calibrated using pH buffer solutions 4.00 ± 0.02 and 7.00 ± 0.02 (Fisher Scientific, Pittsburgh, PA). Sterile DI water (pH = 6.0) was used as a control and was measured at each time period.

2.3.3. Ion release profiles

Each sample ($n = 3$) was immersed in 10 ml of DI water for 1, 7 and 30 days prior to testing. The ion release profile of each specimen was measured using atomic absorption spectroscopy (AAS) on a Perkin-Elmer Analyst 800 (Perkin Elmer, MA, USA). AAS calibration standards for Sr and Zn elements were prepared from a stock solution (Sigma-Aldrich, Oakville, ON, Canada) on a gravimetric basis. Three target calibration standards were prepared for each ion and DI water was used as a control. Owing to the much greater expected concentration of ions, samples were diluted in DI water at 1:10 ratio. The final cumulative concentration was calculated from the results of the measurements taking into account the dilution factor.

3. Results and discussion

3.1. Glass structural and thermal characterization

X-ray diffraction patterns were recorded for each of the formulated glasses and are presented in Fig. 1. XRD confirmed that all fired glasses were fully amorphous; that no crystalline species are present in either *TA0*, *TA1* or *TA2* during glass forming. The results presented herein indicate that any changes in the properties of the glasses will be attributed to Ta$_2$O$_5$ incorporation rather than phase changes/separation in the glasses.
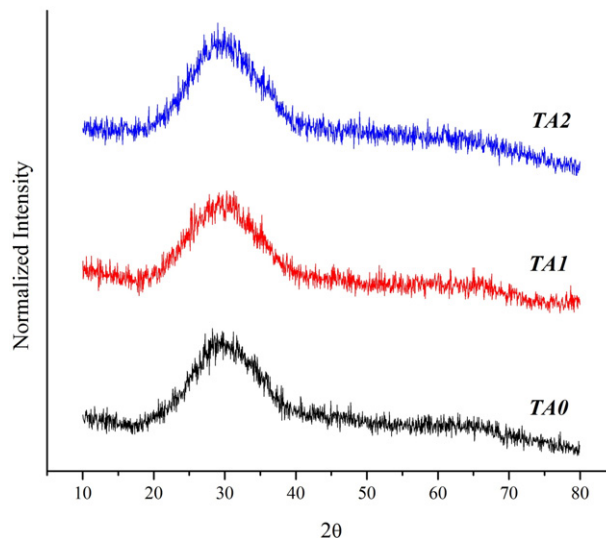

Fig. 1. XRD traces for the formulated glasses.

Particle size analysis (PSA) was conducted for each glass composition and the results are presented in Table 2. The PSA results were comparable for all glasses under study implying that any changes through the series would be related to chemistry, not physicality, of the glasses.

SEM was employed to provide compositional contrast images that result from different atomic number elements and their distribution within the glasses. EDS analysis was also performed to provide qualitative spectra and quantitative relative proportions (wt%) of the particular elements from the SEM backscattered images. SEM-EDS results of the glass series are presented in Fig. 2a–c which show similar morphology for the glasses through the series. Thus, the incorporation of Ta$_2$O$_5$ did not cause any obvious changes in the morphology or the mean particle size of the glass series. The white square in the SEM images (Fig. 2a–c) indicate the interfacial regions used to identify the corresponding EDS spectra as well as the chemical composition ($n = 3$) of the glass series. Qualitative EDS spectra showed that *TA0* contains Si, Zn, Ca, Sr, and P, while *TA1* and *TA2* were found to have the same elements but with the addition of Ta, thus confirming the starting formulation of each glass. Further, it was found, as expected, that Ta increases from 0.0 to 1.9 wt% while Zn decreases from 31.8 to 29.9 wt%, with increasing Ta$_2$O$_5$ content from 0.0 to 2.7 wt%, respectively. The Si fraction however show a significant discrepancy. Si:Zn ratio is ~1:1 in the original glass (wt%, Table 1), however the EDS results show a 1:2 rate. This could be attributed to the high signal present for O and/or the ion diffusion through the glass. Initial quantitative analysis of the glass composition by using EDS can lead to the following assumptions:

– The EDS results are usually collected at low vacuum, therefore the oxygen content recorded by EDS represents BO and NBO and may also represent oxygen in the surrounding environment. This may result in a significant discrepancy in predicting the elemental bulk composition.

– EDS provides the quantitative relative proportions of the particular elements but not the oxides, therefore EDS results cannot be solely used for comparing the chemical composition of the processed and formulated glass.

Table 2
Particle size analysis data for the glass series.

	Average (µm)	d$_{10}$ (µm)	d$_{50}$ (µm)	d$_{90}$ (µm)
TA0	11.5	6.4	8.8	20.2
TA1	11.1	6.4	8.6	18.9
TA2	10.3	6.4	8.4	16.1

(a) TA0

Quantitative EDS	
Element	Wt%
O	41.8
Si	14.4
Zn	31.8
Ca	2.9
Sr	7.8
P	1.5
Ta	0

(b) TA1

Quantitative EDS	
Element	Wt%
O	42.2
Si	14.9
Zn	30.6
Ca	2.7
Sr	7.4
P	1.4
Ta	0.7

(c) TA2

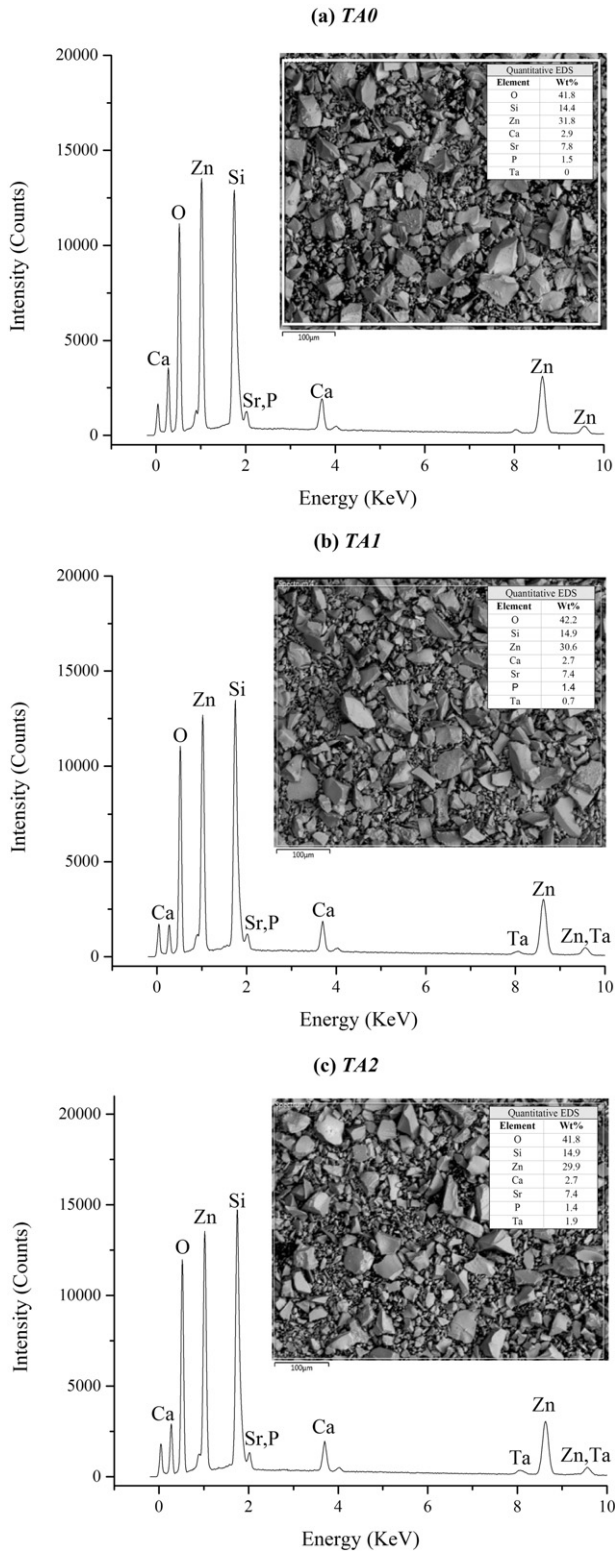| Quantitative EDS	
Element	Wt%
O	41.8
Si	14.9
Zn	29.9
Ca	2.7
Sr	7.4
P	1.4
Ta	1.9

Fig. 2. SEM images of the glass series and the corresponding EDS qualitative spectra and quantitative elemental composition (wt%).

– The penetration depth of the EDS is ~2–5 μm, hence the results also include bulk composition data. This advantage of EDS analysis may however be associated with masking and overlapping issues resulting in significant discrepancy and compositional heterogeneity.

Thermal profiles of the glasses are presented in Fig. 3 DTA curves also shows the recorded thermal events and their assignments. The glass transition temperature was observed at 670 °C, 666 °C and 677 °C for TA0, TA1 and TA2, respectively. Previous studies [6,21] have shown that the addition of transition metals, such as Ta_2O_5, to bio-glasses increases the glass transition temperature (T_g) and facilitates incorporation of the transition metal oxide inside the glass network. The shift in T_g implies increased glass stability, which may be attributed to the formation of BO groups. The glass transition is followed by an exothermic peak caused by glass crystallization (Tc). TA1 and TA2 show an ideal exothermic crystallization reaction at 874 °C and 866 °C, respectively while TA0 shows a broad peak around that region, observed at 897 °C. The slow crystallization of TA0 can be attributed to 'interfering' nucleation and oxidation transitions as well as the slow diffusion rates of the reactants in TA0. This is in good agreement with our previous study where higher levels of Ta_2O_5 resulted in a greater glass forming tendency and a delay in the nucleation process [6]. Finally the melting temperature for TA0 appears at 1094 °C. For TA1 and TA2, endothermic peaks appeared at 1085 °C and 1098 °C, respectively. This last endothermic process for TA1 and TA2 was assigned to initial decomposition and melting of some of the glass elements since the temperature difference does not decrease significantly, compared to that of TA0 at 1094 °C, over the course of the peak. The glass melting temperature of TA1 and TA2 was not observed in this study, agreeing with our previous work which indicated that substituting ZnO with Ta_2O_5 increased melting temperature [6]. This may indicate increased stability and homogeneity of the glass reactants. This assumption agrees with the previous study on similar glass compositions [6]. In that article, results from simultaneous thermal analysis (STA) showed that increasing Ta_2O_5 content at the expense of ZnO resulted in higher glass stability resulting from increased glass transition, crystallization and melting temperatures.

X-ray photoelectron spectroscopy was employed to derive information on the elemental composition and speciation of matter by assessing the electronic structure of the atoms residing within the surface region of the matter being analyzed. The survey spectrum of the glasses formulated is shown in Fig. 4. Besides the expected Si2p, Zn2p3, P2p, Ca2p, Sr3d5, Ta4d and O1s peaks, a C1s peak can be seen in the survey scans which is attributed to 'adventitious carbon' present due to the adsorption of impurities during the glass firing process. It is, however, important to note that the presence of this peak is common and does not affect the interpretation of our results. The XPS survey scan results (Fig. 4) are in good agreement with EDS data. TA0 was found to contain Si2p, Zn2p3, P2p, Ca2p, Sr3d5, and O1s, while TA1 and TA2 contain each of these elements in addition to Ta4d, reflecting the initial glass formulation.

Elemental compositions of the O1s, Si2p, Zn2p3, P2p, Ca2p, Sr3d5, and Ta4d peaks are presented in Table 3. Presenting the elemental composition of the C1s peak can make it difficult to compare relative changes between EDS and XPS results, therefore the elemental composition of the C1s peak is not presented. The elemental composition of all other peaks was adjusted accordingly. Comparing the glass composition obtained from both EDS and XPS with the initial batch formulation (Table 1), it is clear that XPS gives better approximation, particularly when comparing the Ta, Zn and Si content. The wt% of Si and Zn are almost equal in the expected glass compositions (Table 1) to those from the XPS results whereas the EDS quantitative analysis showed a Zn content that is almost twice as large as that of the Si. Further, EDS and XPS show that Ta and O content increases while the content of Zn decreases as a function of Ta_2O_5, thus they present a similar trend to the precursor glass formulations. It is important to note that XPS is a surface technique and therefore explanations offered around the glass composition are subject to the assumption that the bulk of the glass is similar in composition of the surface. However, although EDS quantitative analysis considers the bulk composition of the glass, XPS results record compositions closer to those from the initial batch calculation.

High resolution O1s spectra were also obtained from XPS to determine the effect of Ta_2O_5 substitution. The O1s spectra were curve fitted
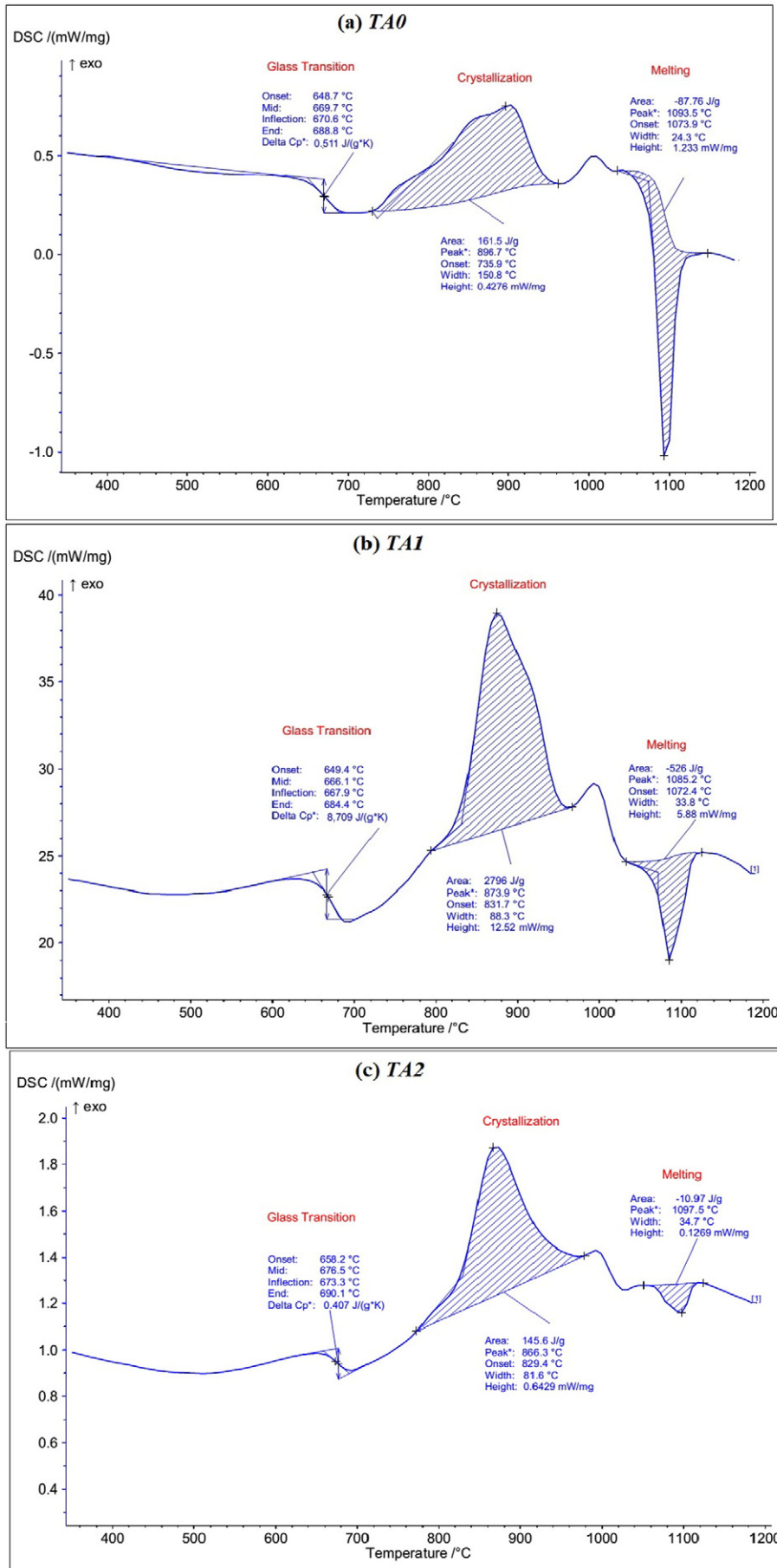
(a) TA0

DSC /(mW/mg)

↑ exo

Glass Transition

Onset: 648.7 °C
Mid: 669.7 °C
Inflection: 670.6 °C
End: 688.8 °C
Delta Cp*: 0.511 J/(g*K)

Crystallization

Melting

Area: -87.76 J/g
Peak*: 1093.5 °C
Onset: 1073.9 °C
Width: 24.3 °C
Height: 1.233 mW/mg

Area: 161.5 J/g
Peak*: 896.7 °C
Onset: 735.9 °C
Width: 150.8 °C
Height: 0.4276 mW/mg

Temperature /°C

(b) TA1

DSC /(mW/mg)

↑ exo

Crystallization

Glass Transition

Onset: 649.4 °C
Mid: 666.1 °C
Inflection: 667.9 °C
End: 684.4 °C
Delta Cp*: 8,709 J/(g*K)

Melting

Area: -526 J/g
Peak*: 1085.2 °C
Onset: 1072.4 °C
Width: 33.8 °C
Height: 5.88 mW/mg

Area: 2796 J/g
Peak*: 873.9 °C
Onset: 831.7 °C
Width: 88.3 °C
Height: 12.52 mW/mg

[1]

Temperature /°C

(c) TA2

DSC /(mW/mg)

↑ exo

Crystallization

Melting

Area: -10.97 J/g
Peak*: 1097.5 °C
Width: 34.7 °C
Height: 0.1269 mW/mg

Glass Transition

Onset: 658.2 °C
Mid: 676.5 °C
Inflection: 673.3 °C
End: 690.1 °C
Delta Cp*: 0.407 J/(g*K)

Area: 145.6 J/g
Peak*: 866.3 °C
Onset: 829.4 °C
Width: 81.6 °C
Height: 0.6429 mW/mg

[1]

Temperature /°C

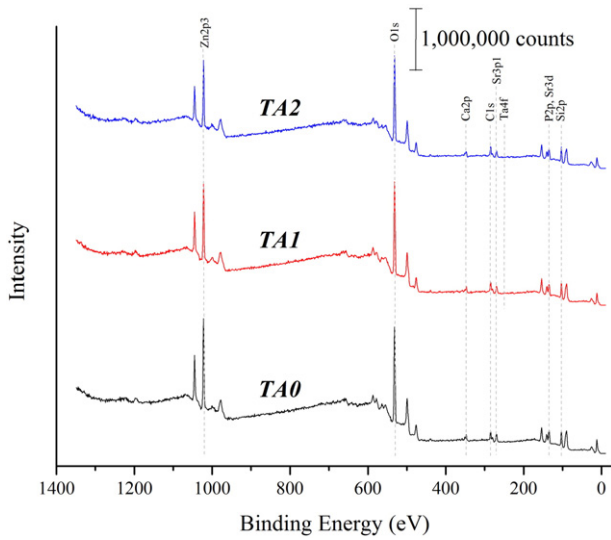**Fig. 3.** DTA curves of the glass series.

Fig. 4. XPS survey scan of the glass series.

Table 3
Elemental composition (wt%) of the glass series as determined by XPS.

	O1s	Si2p	Zn2p3	Ca2p	Sr3p1	P2p	Ta4d
TA0	37.7	23.3	26.9	3.0	7.8	1.4	0.0
TA1	38.1	23.5	24.9	2.9	7.5	1.1	1.6
TA2	38.3	23.9	23.2	2.8	7.1	1.1	3.0

with respect to BO and NBO contributions and are presented in Fig. 5. It is clear from Fig. 5 that the binding energy of the O1s spectrum shifts slightly from 531.8 to 532.1 eV, as a function of Ta_2O_5 content. This is indicative of increasing the BO content in the glass, further suggesting that tantalum acts as a network former in these glasses. Table 4 presents the peak positions for the BO and the NBO and their corresponding atomic % (at%). BO and NBO remained at 531.3 eV and 532.5 eV regardless of Ta_2O_5 content. However increasing Ta_2O_5 content was found to increase the at% of BO peaks on the expense of NBO content, thus increasing the BO/NBO ratio. This aligns with our explanations in the previous article [6], in which we show that Ta acts as a glass former, resulting in increased network connectivity. These results also suggest decreased bioactivity, as the Ta_2O_5 content increases, resulting from the formation of additional Si—O—BO that are known to have a negative effect on the ion exchange process. The solubility section of this article will provide more detailed information with regard to this hypothesis.

MAS-NMR was employed to further investigate the structural effects of Ta_2O_5 incorporation. Chemical shifts in MAS-NMR represents structural changes around the Si atom which lie in the region of −60 to −120 ppm for SiO_4 tetrahedra [22]. Fig. 6 shows the MAS-NMR spectra of the glass series (TA0, TA1 and TA2). Fig. 7a–c are the expanded versions of the NMR spectra of the glass series shown in Fig. 6. Fig. 7d–f are the corresponding curve fitted (simulated) spectra. All glass samples showed similar broad resonances at ~−80 ppm. It can be seen that there are slight chemical shift differences with the chemical shift of TA0 (−80.1) > TA1 (−82.4) > TA2 (−83.5). A shift in ppm in a negative direction, as presented with TA1 and TA2, is indicative of an increase in BO species attached to the silicon, within the glass. Thus confirming with the XPS results presented earlier in this manuscript. Previous studies have indicated that chemical shifts in the region between −60 and
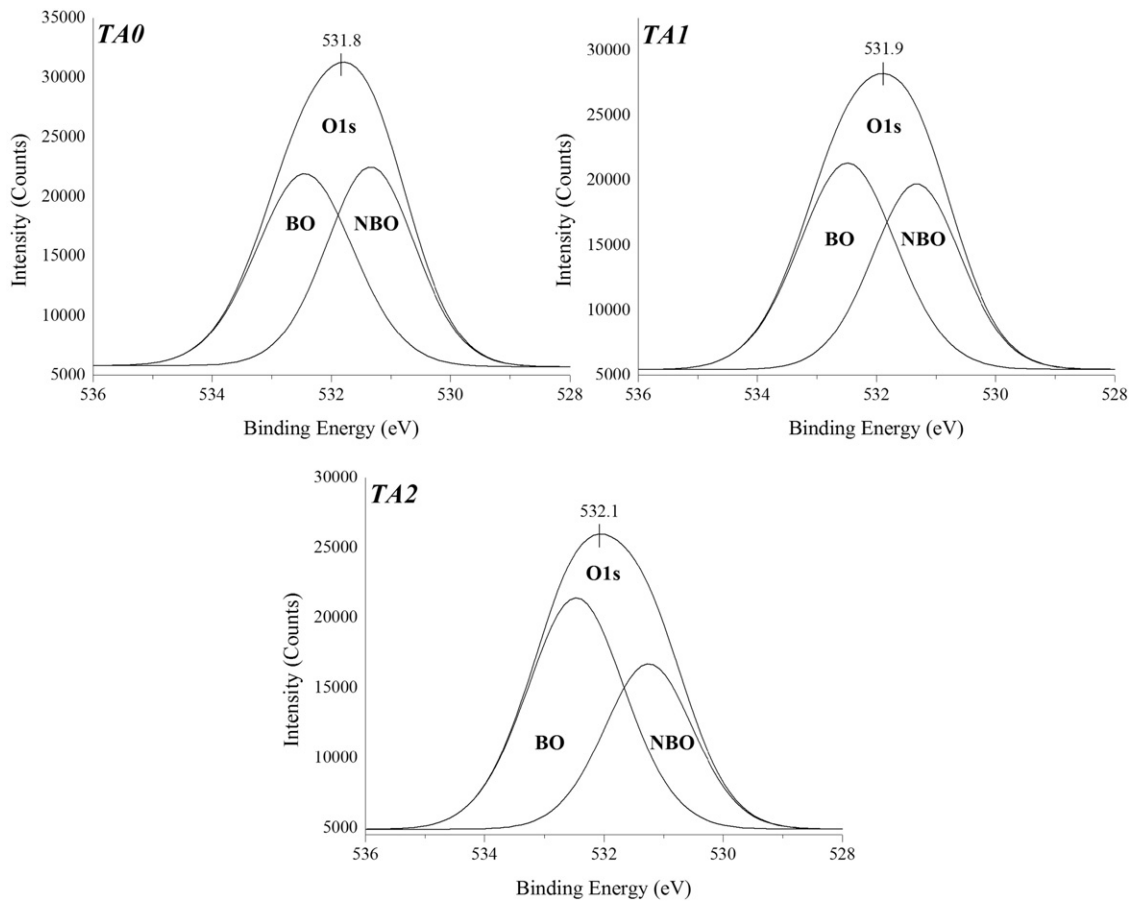

Fig. 5. Curve fitting of the O1s spectra for the glass series with respect to BO and NBO contributions.

Table 4
Peak positions (eV) for the BO and the NBO peaks and their corresponding at%, obtained from the curve fitting of the O1s peak, of the glass series.

	TA0	TA1	TA2
O1s (NBO)	531.3	531.3	531.3
at%	45.2	45.2	39.6
O1s (BO)	532.5	532.5	532.5
at%	54.8	54.8	60.4

−120 ppm represent structural changes around the Si atom in a four coordinate state and suggested the presence of Q^1, Q^2 and Q^3 species at −78, −85 and −95 ppm respectively [22]. All glasses show a broad peak around −80 ppm. This suggests that the formulated glasses contain both Q^1/Q^2. However the broadness of the spectral envelope in all peaks suggests the presence of multiple Q-species and indicates that silicon is present in distorted environments within the glass structure.

3.2. Glass solubility properties

As discussed, substituting Ta_2O_5 with ZnO resulted in increased BO/NBO ratio which correlated with a shift in the thermal events in these glasses to higher temperatures. However, incorporation of Ta_2O_5, replacing ZnO, was found to increase the cumulative % weight loss per unit area of the glasses under study (see Fig. 8a). The results of pH measurements (Fig. 8b) as well as ion release studies of Zn^{2+} and Sr^{2+} ions (Fig. 9a, b) reflected the degradation behavior of the glasses. It can be noted that the TA2 formulation exhibits greater cumulative % weight loss, pH values and cumulative Zn^{2+} and Sr^{2+} ion concentration over a period of 30 days of maturation, when compared to TA1 and/or TA0 glasses. Tables 5 and 6 show the statistics around these studies, which consider both the effect of Ta_2O_5 content and aging on the obtained results. Significant differences (Table 5, $p < 0.05$) in the cumulative % weight loss could only be observed when comparing 1 day with 30 day results for TA0 and TA2 samples. However, no significant difference (Table 6, $p > 0.05$) in the cumulative % weight loss was observed when results were compared with respect to Ta_2O_5 content. Significant changes (Table 5, $p < 0.05$) in the pH measurements were obtained when results were compared with respect to all time modalities. With regard to Ta_2O_5 content, there were significant differences in pH measurements (Table 6, $p < 0.05$) between TA0 and TA1 measured at day 7

and between TA0 and TA2 measured at 7 and 30 days. Ion release studies of both Zn^{2+} and Sr^{2+} showed significant differences ($p < 0.05$) when results were compared with respect to aging time as well as Ta_2O_5 content (see Tables 5 and 6).

Considering the former role of Ta_2O_5 and its substitution with ZnO in the formulated glasses, the solubility properties were expected to decrease. This assumption can be attributed to the fact that dissolution rates must decrease with additional cross-links formed between the silicate groups and tantalum ions. The solubility behavior of the glasses under study however shows that water can diffuse into the glass structure causing some cations to release into the surrounding medium, resulting in increased % weight loss and consequently higher pH and ion release profiles. Previous studies [23,24] have shown that solubility of a glass system strongly depends on the glass composition. It can be generalized that the addition of network modifiers disrupts bonds within the glass network resulting in increased number of NBOs and subsequently increased hydration/solubility when aged in a medium such as water or simulated body fluid. Vice versa, the addition of a glass former results in the formation of additional cross-linking within the glass structure resulting in increased network connectivity, reducing solubility. In this study, the results obtained give a basis for assuming that increasing the Ta_2O_5 content in the formulated silica-based glasses is accompanied by a rapid dissolution of the unstable residual glass phase at the initial stage of the interaction. This could happen due to the physical and chemical characteristics of Ta, which is a basic metal that has a highly reactive surface. The surface of the Ta_2O_5 is protected by a thin oxide layer [25], thus preventing its reaction with water. The authors assume that when Ta_2O_5 is incorporated in a bioglass system and soaked in water, Ta acts in the same way as Ca or Sr, meaning that it acts as an unstable residual glass particle. This results in its quick dissolution in the water upon immersing. Further, the solubility behavior of the glass system under study could have resulted from the fact that Ta is more electropositive than Zn, as predicted from the periodic table of elements. According to the generalized solubility rules, the more electropositive the central atom, the more basic the oxide. The results obtained herein confirm with the general rules of solubility and show that Ta when compared to Zn is a more electropositive metal that increases pH of the medium in which it is immersed due to its rapid dissolution in the surrounding medium. This initial burst of the cations could be favorable for both cell viability and osseo-integration as well as for fighting against bacterial species.

4. Conclusions

The work herein has shown that the synthesis of amorphous Ta_2O_5-containing glasses was possible via the melt-quenching process. The incorporation of up to 0.5 mol% Ta_2O_5 at the expense of ZnO resulted in structural changes resulting from the insertion of TaO units into the silicate network. Glass solubility experiments showed that minor amounts of Ta incorporation altered the glass solubility. The ability to control glass solubility by minor compositional modifications offers great promise for the clinical applications of such bioglasses where the coordination of material solubility with bone remodelling/formation are of paramount importance.
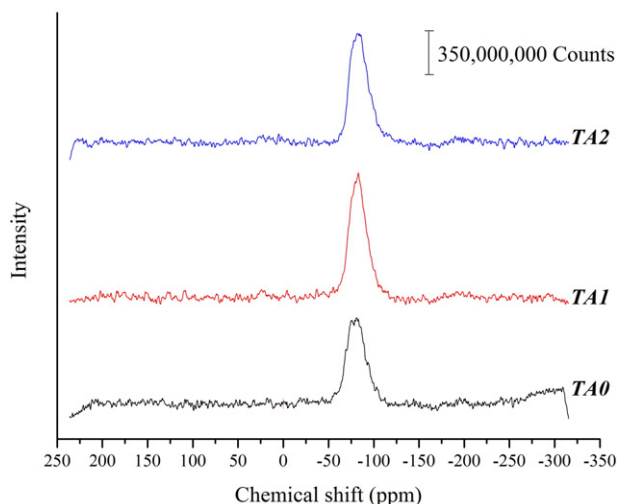

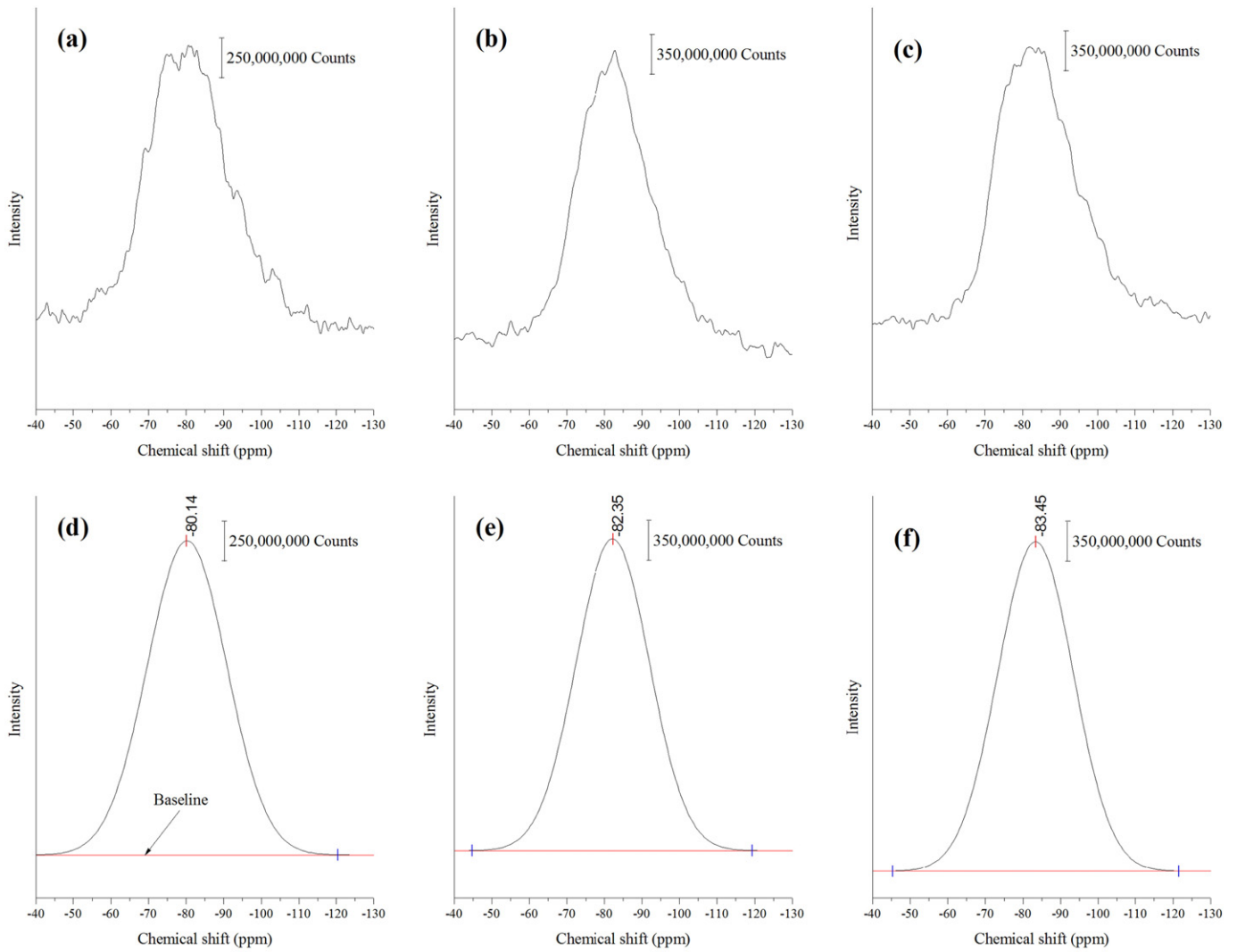**Fig. 6.** ^{29}Si MAS-NMR spectra of the glass series.

Fig. 7. Curve fitting of the ^{29}Si NMR spectra: (a) expanded spectrum of *TA0*; (b) expanded spectrum of *TA1*; (c) expanded spectrum of *TA2*; (d) simulated (curve fitted) spectrum of (a); (e) simulated spectrum of (b) and (f) simulated spectrum of (c).
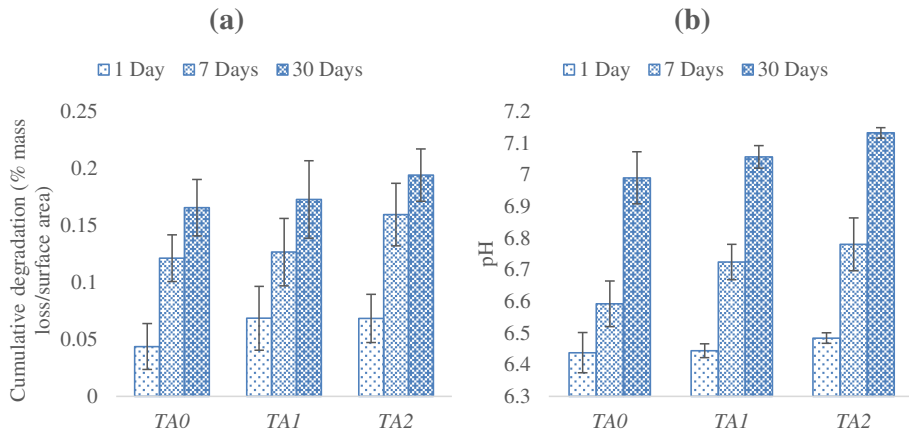

Fig. 8. (a) Percentage weight loss of the glass series in deionized water as a function of time, (b) pH measurements during glass solubility in deionized water. Error bars represent standard deviation from the mean.
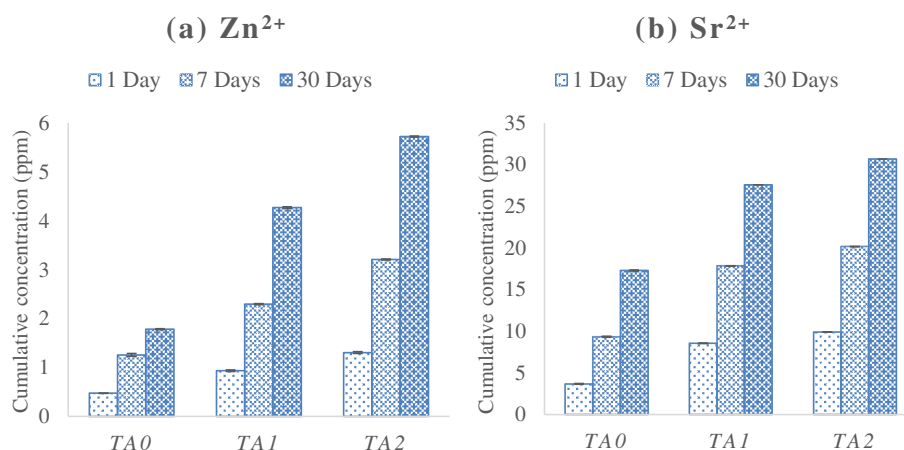
(a) Zn²⁺   **(b) Sr²⁺**

Fig. 9. Ion release profiles of (a) Zn^{2+} and (b) Sr^{2+} ions during glass solubility in deionized water. Error bars represent standard deviation from the mean.

Table 5
Glass solubility statistics (with respect to aging time).

		TA0	TA1	TA2
% weight loss	1 day vs. 7 day	0.082	0.615	0.059
	7 day vs. 30 day	0.536	0.921	0.984
	1 day vs. 30 day	0.006*	0.099	0.009*
pH	1 day vs. 7 day	0.018*	0.000*	0.000*
	7 day vs. 30 day	0.000*	0.000*	0.000*
	1 day vs. 30 day	0.000*	0.000*	0.000*
Sr ion release	1 day vs. 7 day	0.000*	0.000*	0.000*
	7 day vs. 30 day	0.000*	0.000*	0.000*
	1 day vs. 30 day	0.000*	0.000*	0.000*
Zn ion release	1 day vs. 7 day	0.001*	0.000*	0.000*
	7 day vs. 30 day	0.018*	0.000*	0.000*
	1 day vs. 30 day	0.000*	0.000*	0.000*

* The mean difference is significant at the 0.05 level.

Acknowledgment

Table 6
Glass solubility statistics (with respect to Ta_2O_5 content).

		TA0 vs. TA1	TA1 vs. TA2	TA0 vs. TA2
% weight loss	1 day	1.000	1.000	1.000
	7 day	1.000	1.000	0.965
	30 day	1.000	1.000	1.000
pH	1 day	1.000	0.417	0.280
	7 day	0.038*	0.716	0.004*
	30 day	0.212	0.124	0.003*
Sr ion release	1 day	0.000*	0.000*	0.000*
	7 day	0.000*	0.001*	0.000*
	30 day	0.000*	0.001*	0.000*
Zn ion release	1 day	0.001*	0.005*	0.000*
	7 day	0.000*	0.000*	0.000*
	30 day	0.000*	0.000*	0.000*

* The mean difference is significant at the 0.05 level.

References

[1] A. Hoppe, N.S. Guldal, A.R. Boccaccini, A review of the biological response to ionic dissolution products from bioactive glasses and glass-ceramics, Biomaterials 32 (2011) 2757–2774, http://dx.doi.org/10.1016/j.biomaterials.2011.01.004.

[2] J.R. Jones, Review of bioactive glass: from hench to hybrids, Acta Biomater. 9 (2013) 4457–4486, http://dx.doi.org/10.1016/j.actbio.2012.08.023.

[3] W.H. Zachariasen, The atomic arrangement in glass, J. Am. Chem. Soc. 54 (1932) 3841–3851, http://dx.doi.org/10.1021/ja01349a006.

[4] S. Grabowsky, M.F. Hesse, C. Paulmann, P. Luger, J. Beckmann, How to make the ionic Si—O bond more covalent and the Si—O—Si linkage a better acceptor for hydrogen bonding, Inorg. Chem. 48 (2009) 4384–4393, http://dx.doi.org/10.1021/ic900074r.

[5] S.-P. Szu, L.C. Klein, M. Greenblatt, Effect of precursors on the structure of phosphosilicate gels: ²⁹Si and ³¹P MAS-NMR study, J. Non-Cryst. Solids 143 (1992) 21–30, http://dx.doi.org/10.1016/S0022-3093(05)80548-4.

[6] A.M.F. Alhalawani, M.R. Towler, The effect of ZnO ↔ Ta₂O₅ substitution on the structural and thermal properties of SiO₂-ZnO-SrO-CaO-P₂O₅ glasses, Mater. Charact. 114 (2016) 218–224, http://dx.doi.org/10.1016/j.matchar.2016.03.004.

[7] R.T. Sanderson, An interpretation of bond lengths and a classification of bonds, Science 114 (1951) 670–672, http://dx.doi.org/10.1126/science.114.2973.670.

[8] H. Darwish, S. Ibrahim, M.M. Gomaa, Electrical and physical properties of Na₂O–CaO–MgO–SiO₂ glass doped with NdF₃, J. Mater. Sci. Mater. Electron. 24 (2012) 1028–1036, http://dx.doi.org/10.1007/s10854-012-0873-8.

[9] M. Eigen, Structural Chemistry of Glasses, Elsevier, 2002, http://dx.doi.org/10.1016/B978-008043958-7/50030-3.

[10] G. Calas, L. Cormier, L. Galoisy, P. Jollivet, Structure–property relationships in multi-component oxide glasses, C. R. Chim. 5 (2002) 831–843, http://dx.doi.org/10.1016/S1631-0748(02)01459-5.

[11] V.K. Balla, S. Bodhak, S. Bose, A. Bandyopadhyay, Porous tantalum structures for bone implants: fabrication, mechanical and in vitro biological properties, Acta Biomater. 6 (2010) 3349–3359, http://dx.doi.org/10.1016/j.actbio.2010.01.046.

[12] K.B. Sagomonyants, M. Hakim-Zargar, A. Jhaveri, M.S. Aronow, G. Gronowicz, Porous tantalum stimulates the proliferation and osteogenesis of osteoblasts from elderly female patients, J. Orthop. Res. 29 (2011) 609–616, http://dx.doi.org/10.1002/jor.21251.

[13] V.K. Balla, S. Bose, N.M. Davies, A. Bandyopadhyay, Tantalum—a bioactive metal for implants, JOM 62 (2010) 61–64, http://dx.doi.org/10.1007/s11837-010-0110-y.

[14] T. Miyaza, H.-M. Kim, T. Kokubo, C. Ohtsuki, H. Kato, T. Nakamura, Mechanism of bonelike apatite formation on bioactive tantalum metal in a simulated body fluid, Biomaterials 23 (2002) 827–832.

[15] Y.-Y. Chang, H.-L. Huang, H.-J. Chen, C.-H. Lai, C.-Y. Wen, Antibacterial properties and cytocompatibility of tantalum oxide coatings, Surf. Coat. Technol. 259 (2014) 193–198, http://dx.doi.org/10.1016/j.surfcoat.2014.03.061.

[16] M. Roy, V.K. Balla, S. Bose, A. Bandyopadhyay, Comparison of tantalum and hydroxyapatite coatings on titanium for applications in load bearing implants, Adv. Eng. Mater. 12 (2010) B637–B641, http://dx.doi.org/10.1002/adem.201080017.

[17] J. Black, Biologic performance of tantalum, Clin. Mater. 16 (1994) 167–173, http://dx.doi.org/10.1016/0267-6605(94)90113-9.

[18] F. ElBatal, G. El-Bassyouni, Bioactivity of Hench bioglass and corresponding glass-ceramic and the effect of transition metal oxides, SILICON 3 (2011) 185–197, http://dx.doi.org/10.1007/s12633-011-9095-6.

[19] L. Cordeiro, R.M. Silva, G.M. de Pietro, C. Pereira, E.A. Ferreira, S.J.L. Ribeiro, et al., Thermal and structural properties of tantalum alkali-phosphate glasses, J. Non-Cryst. Solids 402 (2014) 44–48, http://dx.doi.org/10.1016/j.jnoncrysol.2014.05.015.

[20] K.M. Wetherall, P. Doughty, G. Mountjoy, M. Bettinelli, A. Speghini, M.F. Casula, F. Cesare-Marincola, E. Locci, The atomic structure of niobium and tantalum containing borophosphate glasses, J. Phys. Condens. Matter. 21 (2009) 37.

[21] T. Kosuge, Y. Benino, V. Dimitrov, R. Sato, T. Komatsu, Thermal stability and heat capacity changes at the glass transition in K_2O–WO_3–TeO_2 glasses, J. Non-Cryst. Solids 242 (1998) 154–164, http://dx.doi.org/10.1016/S0022-3093(98)00800-X.

[22] A. Stamboulis, R.V. Law, R.G. Hill, Characterisation of commercial ionomer glasses using magic angle nuclear magnetic resonance (MAS-NMR), Biomaterials 25 (2004) 3907–3913, http://dx.doi.org/10.1016/j.biomaterials.2003.10.074.

[23] D.S. Brauer, C. Rüssel, J. Kraft, Solubility of glasses in the system P_2O_5–CaO–MgO–Na_2O–TiO_2: experimental and modeling using artificial neural networks, J. Non-Cryst. Solids 353 (2007) 263–270, http://dx.doi.org/10.1016/j.jnoncrysol.2006.12.005.

[24] N.Y. Mikhailenko, E.E. Stroganova, N.V. Buchilin, Solubility of calcium phosphate glasses and glass ceramic materials in water and physiological media, Glas. Ceram. 70 (2013) 158–163, http://dx.doi.org/10.1007/s10717-013-9531-8.

[25] G. Mohandas, N. Oskolkov, M.T. McMahon, P. Walczak, M. Janowski, Porous tantalum and tantalum oxide nanoparticles for regenerative medicine, Acta Neurobiol. Exp. (Wars) 74 (2014) 188–196.